

Applicability of the thin-film approximation in terahertz photoconductivity measurements

Jens Neu, Kevin P. Regan, John R. Swierk, and Charles A. Schmuttenmaer

Citation: *Appl. Phys. Lett.* **113**, 233901 (2018); doi: 10.1063/1.5052232

View online: <https://doi.org/10.1063/1.5052232>

View Table of Contents: <http://aip.scitation.org/toc/apl/113/23>

Published by the [American Institute of Physics](#)

Articles you may be interested in

[Tunable near-infrared perfect absorber based on the hybridization of phase-change material and nanocross-shaped resonators](#)

Applied Physics Letters **113**, 231103 (2018); 10.1063/1.5063481

[Multipolar-interference-assisted terahertz waveplates via all-dielectric metamaterials](#)

Applied Physics Letters **113**, 201103 (2018); 10.1063/1.5063603

[Enhanced photoresponses of an optically driven VO₂-based terahertz wave modulator near percolation threshold](#)

Applied Physics Letters **113**, 231104 (2018); 10.1063/1.5050681

[Noise characterization of patch antenna THz photodetectors](#)

Applied Physics Letters **113**, 161105 (2018); 10.1063/1.5051580

[Imaging and visualization of the polarization state of the probing beam in polarization-sensitive optical coherence tomography](#)

Applied Physics Letters **113**, 231101 (2018); 10.1063/1.5050208

[Electrical tuning of metal-insulator-metal metasurface with electro-optic polymer](#)

Applied Physics Letters **113**, 231102 (2018); 10.1063/1.5054964



Measure Ready
M91 FastHall™ Controller

A revolutionary new instrument
for complete Hall analysis

Lake Shore
CRYOTRONICS

Applicability of the thin-film approximation in terahertz photoconductivity measurements

Jens Neu,^{1,a),b)} Kevin P. Regan,^{1,2,a)} John R. Swierk,² and Charles A. Schmuttenmaer^{1,2,c)}

¹Department of Chemistry, Yale University, New Haven, Connecticut 06520-8107, USA

²Energy Science Institute, Yale University, New Haven, Connecticut 06520-8107, USA

(Received 15 August 2018; accepted 4 November 2018; published online 4 December 2018)

Thin mesoporous photoconductive layers are critically important for efficient water-spitting solar cells. A detailed understanding of photoconductivity in these materials can be achieved via terahertz transient absorption measurements. Such measurements are commonly interpreted using the thin-film approximation. We compare this approximation with a numerical solution of the transfer function without approximations using experimental results for thin-film mesoporous tin oxide (SnO₂) samples which range in thickness from 3.3 to 12.6 μm. These samples were sensitized with either a ruthenium polypyridyl complex or a porphyrin dye. The two sensitizers have markedly different absorption coefficients, resulting in penetration depths of 15 μm and 1 μm, respectively. The thin-film approximation results are in good agreement with the numerical work-up for the short penetration length dye. For the longer penetration length samples, the thin-film formula fails even for thicknesses of only 3 μm ≈ λ/100. The imaginary part of the conductivity calculated using the thin-film formula was significantly larger in magnitude than the value without approximations. This discrepancy between the commonly used thin-film approximation and the numerical solution demonstrates the need for a careful analysis of the thin-film formula. *Published by AIP Publishing.*
<https://doi.org/10.1063/1.5052232>

The sun is the largest energy source available to humankind and research towards harvesting this energy is crucially important. One feasible option is found in water-splitting dye sensitized photoelectrochemical cells (WS-DSPECs) that use solar energy to renewably produce chemical fuels.^{1–6} A critical component of WS-DSPECs is the photoanode material, which consists of a wide bandgap metal oxide material that has a photoabsorbing dye attached to its surface. In the dark, the metal oxide material is an insulator, yet when the dye molecule is photoexcited, it can transfer its excited state electron into the conduction band of the metal oxide material.^{4,7} The metal oxide allows the transport of the photogenerated charges, which travel through the porous nanoparticulate metal oxide film until being transported to a dark cathode to facilitate a proton reduction reaction to generate H₂. Understanding this transport mechanism, and in particular, carrier mobility and lifetime, is crucial for the optimization of WS-DSPECs.

Terahertz (THz) radiation has proven to be an excellent tool for studying photoexcited electron dynamics in photoanode materials.^{7–13} THz radiation provides a noncontact electrical probe that monitors the concentration of free carriers in the system and their associated charge mobility. Since the THz electric field is measured coherently, both amplitude and phase information in the frequency-domain is obtained. As a result, the complex-valued, frequency-dependent refractive index of the photoexcited sample, n_p , at a particular time delay, t_{pump} , after photoexcitation can be determined. Previous publications have used the thin-film approximation.^{7–11} This approximation

was originally designed for microwave spectroscopy on thin superconductive layers.¹⁴ Application of this formula to THz studies of photoexcited layers is common in the field. In this letter, we compare this approximation with non-approximated, computationally expensive calculations of n_p .

For this study, two different photosensitizers were anchored on mesoporous SnO₂, 5-(4-methoxycarbonylphenyl)-10,15,20-tris(2,4,6-trimethylphenyl)-porphyrin (referred to as porphyrin) and (4,4'-diphosphonato-2,2'-bipyridine)bis(2,2'-bipyridine)ruthenium(II) bromide (which is referred to as RuP). Their structures are shown in the [supplementary material](#). These samples were prepared following previously published techniques,^{15,16} and a screen-printed paste of SnO₂ was prepared as described previously.^{3,4,10} The deposition of the layer and sensitization was repeated one, three, and five times, resulting in a total layer thickness of 3.3 μm ± 0.3 μm, 8.2 μm ± 0.3 μm, and 12.6 μm ± 1.0 μm, respectively.

The absorption spectra are shown in Fig. 1. The two sensitizers are markedly different, with porphyrin exhibiting a strong Soret band absorption on the order of 10⁵ M⁻¹ cm⁻¹, while the molar extinction coefficient for the metal to ligand

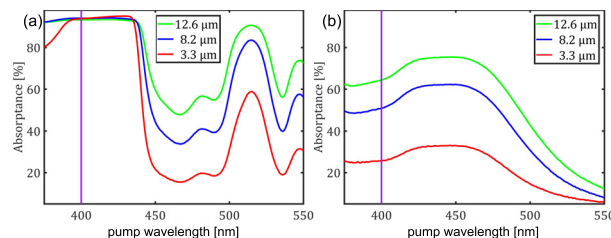


FIG. 1. The optical absorption of (a) porphyrin/SnO₂ and (b) RuP/SnO₂ of thickness of 3.3 μm ± 0.3 μm, 8.2 μm ± 0.3 μm, and 12.6 μm ± 1.0 μm, respectively. The vertical purple line marks the pump wavelength of the photoexcitation (400 nm) used in the THz experiments.

^{a)}J. Neu and K. P. Regan contributed equally to this work.

^{b)}Electronic mail: jens.neu@yale.edu

^{c)}Electronic mail: charles.schmuttenmaer@yale.edu

charge transfer band in RuP is on the order of $10^4 \text{ M}^{-1}\text{cm}^{-1}$.^{17,18} At the wavelength of our pump laser (400 nm), this difference in absorption results in a pump beam penetration depth of $\sim 1 \mu\text{m}$ for porphyrin and of $\sim 15 \mu\text{m}$ for RuP, which is larger than $3.3\text{--}12.6 \mu\text{m}$ of thick SnO_2 films.

The use of these two photosensitizers allows us to access two distinct physical scenarios: The RuP-sensitized SnO_2 films generate charge carriers throughout the full thickness of the films, while the porphyrin-sensitized SnO_2 films exhibit a very thin photoexcited layer on top of a thicker layer of a nonphotoexcited porphyrin/ SnO_2 film (see Fig. 2).

The THz spectrometer has been described in detail in previous publications.^{10,19} In short, the output of a 1 kHz 4 mJ amplifier at 800 nm is split into a pump and a THz generation beam. The generation beam is frequency doubled to 400 nm for photoexcitation; the other beam is used to generate THz radiation via two-color air plasma. Based on previous studies, we chose a pump delay of 1350 ps.¹¹ This delay time is significantly larger than the injection time of ≈ 100 ps, and hence we can assume steady-state behavior of the mobile charges in the conduction band. The measured THz pulses at a particular t_{pump} are Fourier transformed, resulting in the frequency-dependent THz field $E_{\text{pump}}(\omega, t_{\text{pump}})$. Additionally a THz spectrum without photoexcitation is measured and used as a reference, $E_{\text{ref}}(\omega)$, to calculate the spectral transfer function $T_{\text{pump}}(\omega, t_{\text{pump}}) = \frac{E_{\text{pump}}(\omega, t_{\text{pump}})}{E_{\text{ref}}(\omega)}$.

Figure 2 presents a schematic diagram of the samples. The reference sample is not photoexcited, in the RuP-sensitized sample, the entire film is photoexcited, and in the porphyrin-sensitized sample, only a fraction of the film is photoexcited. n_a , n_q , n_n , and n_p are the complex-valued refractive indices of air ($\nu = 1 \text{ THz}$) = 1, fused quartz ($\nu = 1 \text{ THz}$) = 1.95, and non-photoexcited SnO_2 ($\nu = 1 \text{ THz}$) = 2.2 (see [supplementary material](#)), and photoexcited SnO_2 , respectively. For the presented calculations, frequency resolved measured refractive indices are used. d_n is the thickness of the SnO_2 layer and d_p is the thickness of the excited layer, which is equal to d_n in the case of RuP. In the case of porphyrin sensitization, d'_n is the thickness of the non-photoexcited material and d'_p is the thickness of the photoexcited material. It is seen that $d'_n + d'_p = d_n$ (and also d_p). The FP_{ijk} terms account for the Fabry-Perot reflections within a layer of material “j” sandwiched between materials of “i” and “k.” Furthermore, we define the Fresnel reflection coefficient as $r_{ji} = \frac{n_i - n_j}{n_i + n_j}$ and $t_{ij} = 1 + r_{ij}$ and the propagation function as $P_{d,ni} = e^{-id_in_i k_0}$, with the wavevector of vacuum k_0 .

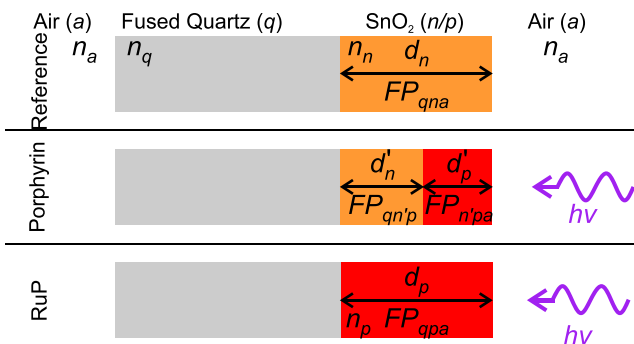


FIG. 2. Schematic representation of the samples investigated.

The quartz substrate is thick enough such that no internal reflections from it are collected. These considerations allow us to define the complex transfer functions of a known input field E_0 for photoexcited or non-photoexcited SnO_2 . The simplest case is non-photoexcited SnO_2 to give the transmission T

$$E_{\text{ref}}(\omega) = E_0 t_{aq} P_{d_q n_q} t_{qn} t_{na} F P_{qna}. \quad (1)$$

The equation for the RuP-sensitized sample is identical except that the quantities for the photoexcited material are used

$$E_{\text{pump}}(\omega) = E_0 t_{aq} P_{d_q n_q} t_{qp} t_{pa} F P_{qpa}. \quad (2)$$

Finally, the most general case of porphyrin-sensitized SnO_2 that has both photoexcited and non-photoexcited layers is given by

$$E_{\text{pump}}(\omega) = E_0 t_{aq} P_{d_q n_q} t_{qn} P_{d_n n_n} t_{np} P_{d_p n_p} t_{pa} F P_{qn'p} F P_{n'pa}, \quad (3)$$

$$F P_{jkl}(\omega) = \sum_{p=0}^M (r_{kl} r_{kj} P_{d_j n_j}^2)^p, \quad (4)$$

$$\lim_{M \rightarrow \infty} (F P_{ijk}(\omega)) = \frac{1}{1 - (r_{kl} r_{kj} P_{d_j n_j}^2)}.$$

All measurable Fabry-Perot reflections are captured within our 6.5 ps THz transient; therefore, the infinite series of reflections reduces to the form shown in the second line of Eq. (4). This infinite sum converges for non-gain natural materials. To calculate the refractive index n_p , Eq. (3) is normalized to a reference measurement through non-photoexcited SnO_2

$$T_{\text{por}} = \frac{t_{aq} P_{d_q n_q} t_{qn} P_{d_n n_n} t_{np} P_{d_p n_p} t_{pa} F P_{qn'p} F P_{n'pa}}{t_{aq} P_{d_q n_q} t_{qn} P_{d_n n_n} t_{na} F P_{qna}} \quad (5)$$

with a similar equation for the RuP-sensitized case where the entire SnO_2 layer is photoexcited. Inserting the Fresnel coefficients and propagation functions yields

$$T_{\text{por}} = \frac{n_p n_n + n_a}{n_n n_p + n_a n_n + n_p} \frac{2n_n}{e^{ik_0 d_p (n_p - n_n)}} \frac{F P_{qn'p} F P_{n'pa}}{F P_{qna}}. \quad (6)$$

Alternatively, if the penetration-depth for the pump beam is larger than the layer thickness (as is the case with RuP/ SnO_2), the complete SnO_2 film is photoexcited and the transfer function is described by

$$T_{\text{RuP}} = \frac{t_{aq} P_{d_q n_q} t_{qp} P_{d_p n_p} t_{pa} F P_{qpa}}{t_{aq} P_{d_q n_q} t_{qn} P_{d_n n_n} t_{na} F P_{qna}}, \quad (7)$$

$$T_{\text{RuP}} = \frac{n_p n_n + n_a n_q + n_n}{n_n n_p + n_a n_q + n_p} e^{ik_0 d_p (n_p - n_n)} \frac{F P_{qpa}}{F P_{qna}}. \quad (8)$$

Equations (6) and (8) are numerically solved to extract n_p . This equation is frequency-dependent and complex-valued. The refractive indices are obtained from the generalized permittivity of the photoexcited sample, the lattice permittivity of the non-photoexcited sample, and the photoconductivity of the photoexcited sample. The lattice permittivity, $\epsilon_{\text{lattice}} \approx n_n^2$, is assumed to be unchanged upon photoexcitation, and it is also assumed that the sample is non-magnetic

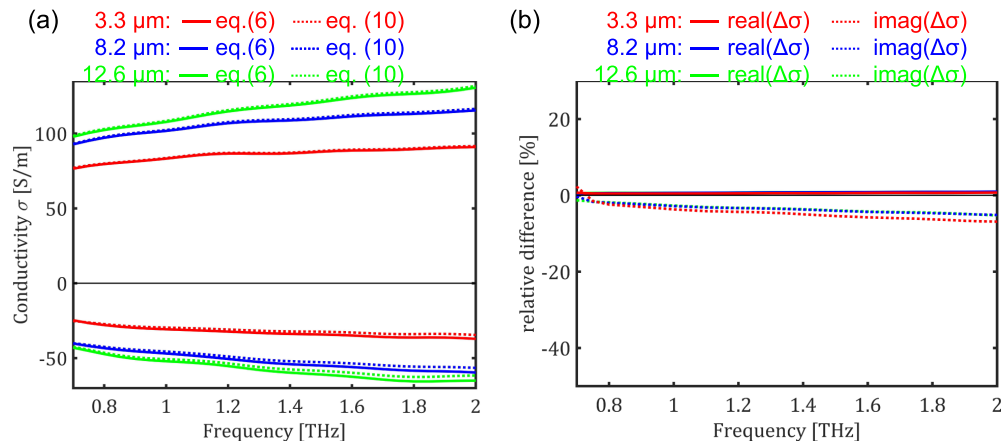


FIG. 3. Terahertz photoconductivity of porphyrin-sensitized SnO_2 . (a) Photoconductivity for porphyrin/ SnO_2 films calculated with the thin-film approximation [dashed lines, Eq. (10)] and the non-approximated numerical solution [solid lines, Eq. (6)]. (b) Percent deviation of the thin-film approximation from the non-approximated numerical solution. The real conductivity is plotted as solid lines and the imaginary conductivity is plotted as dashed lines. The vertical scale is the same as that in Figs. 3(b) and 4(b) to allow for easier comparison.

$$\epsilon_p(\omega, t_{\text{pump}}) = n_p^2 = \epsilon_{\text{lattice}}(\omega) + \frac{i\sigma(\omega, t_{\text{pump}})}{\epsilon_0\omega}. \quad (9)$$

This expression relates the change in the sample's refractive index to a change in the conductivity of the film, $\sigma(\omega, t_{\text{pump}})$. Numerically solving these equations is computationally expensive. Therefore, several previous publications have expanded upon the expression derived by Glover and Tinkham¹⁴ in 1957 for a thin superconducting material, and this is referred to as thin-film approximation.^{10,11,20–22} If the photoexcited layer fulfills $n_p k_0 d_p \ll 1$ and $k_p k_0 d_p \ll 1$, the conductivity is given by^{21,23}

$$\sigma(\omega, t_{\text{pump}}) = \frac{n_n + 1}{Z_0 d_p} \left(\frac{1}{T(\omega, t_{\text{pump}})} - 1 \right), \quad (10)$$

with $Z_0 = 376.7 \Omega$ being the impedance of free space and $T(\omega, t_{\text{pump}})$ the spectral transmission at a given pump delay t_{pump} .

While this equation was originally developed for microwave studies of thin-layer superconductors on insulating substrates, it has been widely used for terahertz spectroscopy of photoexcited materials.^{10,11,20–22}

The primary question addressed in this letter is: what value is considered to be a value much less than 1? Is it 0.5? Or is it 0.1? Or is it 0.01? Therefore, we compare the measured photoconductivity of several samples, ranging from $n_p k_0 d_p = 0.04$ to 0.5, using the thin-film formula [Eq. (10)] and the non-approximated Eqs. (6) and (8).

From Fig. 1(a), it is apparent that porphyrin-sensitized SnO_2 has a very high extinction coefficient at 400 nm. The optical penetration length was determined using an integration sphere to be $d_p \sim 1 \mu\text{m}$, which results in the SnO_2 film not being fully photoexcited, as seen in Fig. 2. Therefore, an additional 2.3 μm (1 layer) to 11.6 μm (5 layers) of nonphotoexcited SnO_2 remains with a refractive index of n_n .

The calculated photoconductivity of the one, three, and five layer porphyrin-sensitized SnO_2 samples using both Eqs. (6) and (10) is plotted in Fig. 3(a). The dashed lines depict the results of using the thin-film approximation [Eq. (10)], and the solid lines represent the non-approximated numerical solution [Eq. (6)]. The percent difference between the two methods is plotted in Fig. 3(b). The results agree within 1%

for the real conductivity, and within 5% for the imaginary conductivity.

Given the small absorption depth for the porphyrin/ SnO_2 samples, the total number of carriers is independent of the layer thickness, and is defined by the pump fluence (which remains constant for all of the measurements). As the overall layer thickness increases, the same number of photoexcited free electrons is generated, and it is seen that the photoconductivity for all three samples is nearly the same.

The conductivity is measured 1350 ps after photoexcitation. This allows the carriers to diffuse into the nonphotoexcited layer which reduces the carrier density in the thickest sample with respect to the thinnest sample. The lower electron density reduces the electron-electron scattering probability.¹¹ As a result, the carrier mobility and lifetime is higher in the thicker layer, and results in an increase in conductivity with increasing layer thickness. While there are small deviations between the two calculations on the order of 1%–5% in the imaginary conductivity, the thin-film approximation nicely reproduces the photoconductivity calculated from the non-approximated method.

The RuP-sensitized SnO_2 sample has an overall optical absorption length of $\sim 15 \mu\text{m}$, which is larger than the thicknesses of the SnO_2 films (3.3–12.6 μm). As seen in Fig. 1(b), even the five layer film does not reach an absorptance higher than 65% when excited at 400 nm. Therefore, the SnO_2 layer will be fully photoexcited and described by the complex photoexcited index of refraction n_p . The photoconductivity calculations of the one, three, and five layer RuP/ SnO_2 samples are plotted in Fig. 4(a). The dashed line depicts the results of using the thin-film approximation [Eq. (10)] and the solid line represents the non-approximated numerical solution [Eq. (8)].

A comparison of Figs. 3 and 4 shows that the photoconductivity in the short absorption length case (porphyrin/ SnO_2) is about an order of magnitude higher than the RuP/ SnO_2 sample. Furthermore, when the two and three layer cases are compared, we note a 15-fold higher conductivity for the porphyrin/ SnO_2 sample, which is caused by the stronger total absorption. The RuP/ SnO_2 sample is thinner than the absorption length so less than 1/e of the pump photons are absorbed. In the case of porphyrin/ SnO_2 , all photons are absorbed, resulting in an approximately 2–3 times higher number of carriers. These carriers are

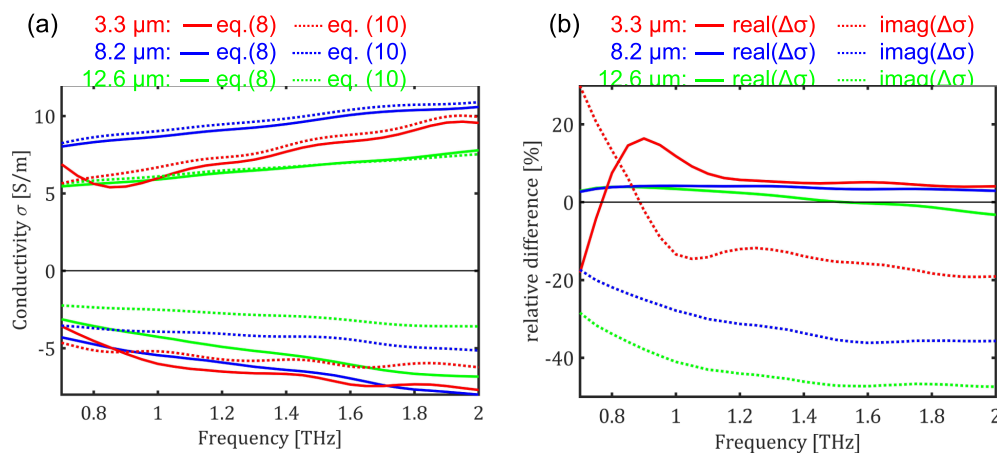


FIG. 4. Terahertz photoconductivity of RuP-sensitized mesoporous SnO_2 . (a) Calculated photoconductivity for RuP/ SnO_2 films with the thin-film approximation [dashed lines, Eq. (10)] and the non-approximated numerical solution [solid lines, Eq. (8)]. (b) Percent deviation of the thin-film approximation from the non-approximated numerical solution. The real conductivity is plotted as solid lines and the imaginary conductivity is plotted as dashed lines. For better comparison, Figs. 3(b) and 4(b) use the same scale.

also confined in a significantly thinner layer ($1\ \mu\text{m}$ versus $12.6\ \mu\text{m}$), which causes a higher carrier density and therefore a higher conductivity.

There is a significant difference in the RuP/ SnO_2 conductivities calculated using the non-approximated numerical solution versus the thin-film approximation. The percent difference between the two methods is plotted in Fig. 4(b). Similar to the case of porphyrin-sensitized SnO_2 , the results for the real part of the photoconductivity agree within 5%, similar to previous results on GaAs.²⁴ However, a very significant change in the imaginary conductivity is noted. The difference between the thin-film approximation and the correct calculation for the thinnest sample with $d_p = 3.3\ \mu\text{m} \approx \lambda/100$ is -10% , for $n_p k_0 d_p \approx 0.1$. It increases with the total layer thickness to reach a maximum of -45% for the $12.6\ \mu\text{m}$ sample, for $n_p k_0 d_p \approx 0.5$.

In conclusion, we have compared the widely used thin-film approximation with a numerical data-workup without any approximations. The difference between the two approaches is demonstrated for mesoporous SnO_2 , sensitized with a dye that results in a short absorption length (porphyrin) or one that results in a long absorption length (RuP). The difference between the two methods is less than 5% if a strong photo absorber is used. In contrast, if a dye with a smaller extinction coefficient (RuP) is used, which thereby leads to a large absorption length, the discrepancy between the calculated conductivities is up to 45%. This large error in the approximation clearly demonstrates that the thin-film formula should be applied with care.

See [supplementary material](#) for the Matlab script used which can be freely downloaded from our homepage at <https://THz.yale.edu>, chemical structure of the used compounds, and the refractive index of non-excited mesoporous SnO_2 .

This work was supported by the Office of Basic Energy Sciences, Division of Chemical Sciences, Geosciences, and Energy Biosciences, Department of Energy, under Contract No. DE-FG02-07ER15909 for the data collection and the National Science Foundation under Grant No. NSF CHE-CSDMA 1465085 for the data analysis, as well as by a generous donation from the TomKat Charitable Trust. We

would like to thank Shin Hee Lee and Jianbing Jiang for providing us with the dyes for sensitization.

- ¹M. K. Brennaman, R. J. Dillon, L. Alibabaei, M. K. Gish, C. J. Dares, D. L. Ashford, R. L. House, G. J. Meyer, J. M. Papanikolas, and T. J. Meyer, *J. Am. Chem. Soc.* **138**, 13085 (2016).
- ²J. Li and N. Wu, *Catal. Sci. Technol.* **5**, 1360 (2015).
- ³J. R. Swierk, N. S. McCool, and T. E. Mallouk, *J. Phys. Chem. C* **119**, 13858 (2015).
- ⁴J. R. Swierk, N. S. McCool, C. T. Nemes, T. E. Mallouk, and C. A. Schmuttenmaer, *J. Phys. Chem. C* **120**, 5940 (2016).
- ⁵K. J. Young, L. A. Martini, R. L. Milot, R. C. Snoberger, V. S. Batista, C. A. Schmuttenmaer, R. H. Crabtree, and G. W. Brudvig, *Coord. Chem. Rev.* **256**, 2503 (2012).
- ⁶W. J. Youngblood, S.-H. A. Lee, K. Maeda, and T. E. Mallouk, *Acc. Chem. Res.* **42**, 1966 (2009).
- ⁷G. M. Turner, M. C. Beard, and C. A. Schmuttenmaer, *J. Phys. Chem. B* **106**, 11716 (2002).
- ⁸R. L. Milot, G. F. Moore, R. H. Crabtree, G. W. Brudvig, and C. A. Schmuttenmaer, *J. Phys. Chem. C* **117**, 21662 (2013).
- ⁹P. Tiwana, P. Docampo, M. B. Johnston, H. J. Snaith, and L. M. Herz, *ACS Nano* **5**, 5158 (2011).
- ¹⁰K. P. Regan, C. Koenigsmann, S. W. Sheehan, S. J. Konezny, and C. A. Schmuttenmaer, *J. Phys. Chem. C* **120**, 14926 (2016).
- ¹¹K. P. Regan, J. R. Swierk, J. Neu, and C. A. Schmuttenmaer, *J. Phys. Chem. C* **121**, 15949 (2017).
- ¹²J. Neu and M. Rahm, *Opt. Express* **23**, 12900 (2015).
- ¹³P. Kužel, F. Kadlec, and H. Němec, *J. Chem. Phys.* **127**, 024506 (2007).
- ¹⁴R. E. Glover and M. Tinkham, *Phys. Rev.* **108**, 243 (1957).
- ¹⁵I. Gillaizeau-Gauthier, F. Odobel, M. Alebbi, R. Argazzi, E. Costa, C. A. Bignozzi, P. Qu, and G. J. Meyer, *Inorg. Chem.* **40**, 6073 (2001).
- ¹⁶H. Imahori, S. Hayashi, T. Umeyama, S. Eu, A. Oguro, S. Kang, Y. Matano, T. Shishido, S. Ngamsinlapasathian, and S. Yoshikawa, *Langmuir* **22**, 11405 (2006).
- ¹⁷K. Hanson, M. K. Brennaman, A. Ito, H. Luo, W. Song, K. A. Parker, R. Ghosh, M. R. Norris, C. R. K. Glasson, J. J. Concepcion, R. Lopez, and T. J. Meyer, *J. Phys. Chem. C* **116**, 14837 (2012).
- ¹⁸J. R. Swierk, D. D. Méndez-Hernández, N. S. McCool, P. Liddell, Y. Terazono, I. Pahk, J. J. Tomlin, N. V. Oster, T. A. Moore, A. L. Moore, D. Gust, and T. E. Mallouk, *PNAS* **112**, 1681 (2015).
- ¹⁹M. C. Beard, G. M. Turner, and C. A. Schmuttenmaer, *Phys. Rev. B* **62**, 15764 (2000).
- ²⁰K. M. B. Murali, L. Man Michael, K. V. Soumya, C. Catherine, H. Takaaki, T.-T. Jaime, T. C. Sekhar, N. Patrick, C. Patricia, N. Narayanan Tharangattu, R. Angel, M. Ajayan Pulickel, T. Saikat, and M. Dani Keshav, *Adv. Opt. Mater.* **3**, 1551 (2015).
- ²¹P. U. Jepsen, D. G. Cooke, and M. Koch, *Laser Photonics Rev.* **5**, 124 (2011).
- ²²C. Larsen, D. G. Cooke, and P. U. Jepsen, *J. Opt. Soc. Am. B* **28**, 1308 (2011).
- ²³J. Lloyd-Hughes and T.-I. Jeon, *J. Infrared, Millimeter, Terahertz Waves* **33**, 871 (2012).
- ²⁴M. C. Beard, G. M. Turner, and C. A. Schmuttenmaer, *J. Appl. Phys.* **90**, 5915 (2001).